JOURNAL OF GUIDANCE, CONTROL, AND DYNAMICS
Vol. 47, No. 6, June 2024

Flexible Quadrotor Unmanned Aerial Vehicles: Spatially Distributed Modeling and Delay-Resistant Control

Emre Eraslan*
University of Illinois at Urbana-Champaign, Champaign, Illinois 61820
and
Yildiray Yildiz†
Bilkent University, 06800 Ankara, Turkey

https://doi.org/10.2514/1.G007665

This paper introduces an analytical framework for the derivation of distributed-parameter equations of motion of a flexible quadrotor. This approach helps obtain rigid and elastic equations of motion simultaneously, in a decoupled form, to facilitate the controller design. A delay-resistant low-frequency adaptive controller is employed, which prevents excessive oscillations due to flexible dynamics, compensates uncertainties, and addresses the inherent time delay. In addition to this, a delay-dependent stability condition for the overall system dynamics is obtained including the human operator with reaction time delay, the adaptive controller, and the flexible quadrotor dynamics with input delay. With comparative simulation studies, it is demonstrated that the flexible arm tip oscillations are significantly reduced when the low-frequency delay-resistant closed-loop reference model adaptive controller is used, compared to a closed-loop reference model adaptive controller and a conventional model reference adaptive controller.

Nomenclature

CRM	=	closed loop reference adaptive contro
CRM-H	=	closed loop reference adaptive control with the human pilot mode
DRCRM	=	delay resistant closed loop reference adaptive contro
DRCRM-H	=	delay resistant closed loop reference adaptive control with human pilot mode
MRAC	=	model reference adaptive contro
MRAC-H	=	model reference adaptive control with the human pilot mode
UAV	=	unmanned aerial vehicle

I. Introduction

QUADROTOR unmanned aerial vehicles (UAVs) are conventionally treated as rigid bodies because most of the time flexible dynamics are negligible. However, for quadrotors that are built using very thin and light materials, flexible dynamics cannot be ignored. The preference of these materials contributes significantly to quadrotor design in terms of 1) lower manufacturing and maintenance costs, 2) reduced battery consumption, 3) reduced fragility due to collision forces, and 4) reduced proneness to damages during vertical landing. Nonetheless, during a flight mission, flexible effects may introduce excessive vibrations, which may result in structural damage to the UAV body. To be able to conduct a careful analysis for these vehicles, a rigorous mathematical model of flexible dynamics is needed.

Research efforts reported in the open literature pertaining to flexible quadrotor UAVs are relatively scarce. In [1], the flexibility of a quadrotor, upon impact with a wall, is formulated as deformation and reconfiguration of the chassis using a revolute spring and a damper. In [2], a structural vibration analysis of a typical quadrotor UAV chassis using experimental and numerical methods is conducted. This analysis is used to find the lowest vibration regions for electrical equipment placement. In [3], structural resonance is attributed to the interference between the excitation frequencies of the propellers and fundamental frequencies of the UAV structure. A model that uses radial basis functions is constructed to approximate the dependency of the first fundamental frequency on structural parameters. This model is used to find the optimum values of the parameters to prevent excitation interference. It is noted that neither [2] nor [3] contains a dynamical model of the quadrotor UAV that can be employed for control design or analysis of the close-loop control system.

The flexible quadrotor UAV model developed in this paper distinguishes itself from the aforementioned earlier studies by providing a fully distributed dynamical model that can be used for control design. A distributed modeling approach for aerospace applications is not new (see [4–7]). In particular, a number of approaches to flexible fixed-wing aircraft design have been proposed, such as aerodynamic strip theory on wings [8], bifurcation and continuation methods [9], nonlinear reduced-order models [10], the interconnected multiple beam structure method [11], and the structural dynamic modeling method [12]. These studies are also extended to very flexible fixed-wing UAVs, in other words, that have long flexible arms [13–15]. However, similar results do not exist for quadrotor UAVs, and transferring the existing results to quadrotor UAVs is not a trivial task. In this paper, we introduce an analytical framework to derive distributed equations of motion of a flexible quadrotor UAV. The applied method is predicated on Lagrangian mechanics using the mean-axes theorem. This approach helps obtain rigid and elastic equations of motion simultaneously, in a decoupled form, which facilitates the controller design.

After deriving the equations of motion, we address the question of control. Controlling flexible quadrotor dynamics requires overcoming several challenges. These include uncertainties, proneness to extensive oscillations due to flexibility, and time delays stemming from 1) response times of motor drives [16], 2) complicated data measurements of various sensors [17], 3) data dropout [18], and 4) problems in communication networks [19]. We adopt the delay-resistant closed-loop reference model adaptive controller (DRCRM) [20] to address these issues. We tailor DRCRM for the state accessible case studied in this paper for two specific scenarios. In the first scenario, the reference command is predefined, whereas a reference that is changing in real time is considered in the second scenario. Through extensive comparative simulation studies using the high-fidelity model developed in this paper, we demonstrate that alternative controllers that do not specifically address the mentioned challenges fail to match the performance of DRCRM. DRCRM

Received 14 April 2023; accepted for publication 29 January 2024; published online 25 March 2024.

*Graduate Research Assistant, Department of Industrial & Enterprise Systems Engineering, 104 S. Mathews Avenue; emree2@illinois.edu.
†Assistant Professor, Department of Mechanical Engineering, Bilkent, Ankara; yyildiz@bilkent.edu.tr.

provides a system response with the lowest-frequency and -amplitude oscillations.

To complete the picture, we derive the stability limits of the overall closed-loop system, consisting of the human operator with a reaction time delay, the controller, and the flexible quadrotor with input delay. Together with the inclusion of the human operator reaction time delay analysis, we fill an important gap in the literature by proposing an overall control framework, where a distributed modeling of flexible quadrotor UAV is developed together with a low-frequency adaptive control implementation and a human-in-the-loop stability analysis including reaction time delays. The involvement of human operator in the overall analysis is especially important to understand the whole cyber physical human system [21–24].

A preliminary version of this work is published at 2021 IEEE Conference on Decision and Control [25]. Different from the conference version, in this paper, we elucidate the modeling of elastic quadrotor dynamics in full detail such as the derivation of orthogonality conditions and the derivation of the temporal part of the flexible dynamics partial differential equations. Furthermore, in the conference version, a delay-free plant dynamics is assumed, and the only delay in the system is the human reaction time delay. In this paper, we remove this assumption by including the inherent time delay in plant dynamics, the sources of which are given in the previous paragraphs.

This paper is organized as follows. Section II presents the modeling of elastic quadrotor dynamics. The controller design and human-in-the-loop stability analysis are given in Sec. III. Simulation results are presented in Sec. IV, and the conclusions are given in Sec. V.

II. Modeling of Elastic Quadrotor Dynamics

We have taken inspiration from the Lagrangian energy-based approach outlined in [6,8] to develop the distributed equations of motion for our model. Unlike the models presented in [6,8], our model takes into account both the energy dissipation effects described in [26,27] and the flexibility of the quadrotor arms. In this section, we first provide the background information necessary to understand the model and then develop the distributed parameter model itself.

A. Dynamics of Unconstrained Elastic Bodies

In an unconstrained elastic body, the inertial position $\mathcal{R}_\mathcal{E}$ of a mass element ρdV where ρ is the density and dV is the infinitesimal volume can be found by adding its position relative to a noninertial body-fixed frame $\mathcal{G}$, denoted as $\mathcal{R}_\mathcal{G}$, and the position of this body reference frame relative to the inertial frame $\mathcal{F}$, denoted as $\mathcal{R}_\mathcal{F}$ (see Fig. 1). This can be expressed as

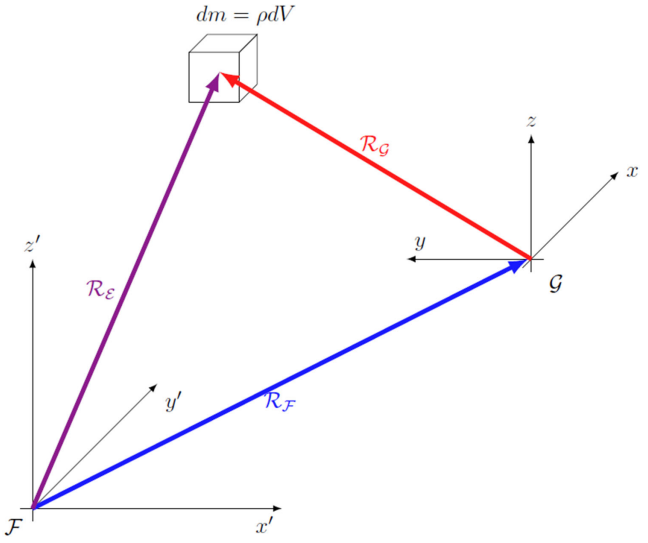

Fig. 1 Position of a mass element with respect to reference frames.

$$\mathcal{R}_\mathcal{E} = \mathcal{R}_\mathcal{F} + \mathcal{R}_\mathcal{G} \tag{1}$$

In the rigid-body formulation, the time rate of change of $\mathcal{R}_\mathcal{G}$ is assumed to be 0 [28,29]. However, this assumption does not hold for the elastic body formulation [6]. We can express the kinetic and potential energy terms, denoted as $\mathcal{T}$ and $\mathcal{U}$, respectively, using the time derivative with respect to $\mathcal{R}_\mathcal{F}$ denoted as $(d/dt)(.)$, the time derivative with respect to $\mathcal{R}_\mathcal{G}$ denoted as $(\delta/\delta t)(.)$, and the angular velocity ω of $\mathcal{R}_\mathcal{G}$ with respect to $\mathcal{R}_\mathcal{F}$. This yields

$$\mathcal{T} = \frac{1}{2}\int_V \left\{ \frac{d\mathcal{R}_\mathcal{F}}{dt}\frac{d\mathcal{R}_\mathcal{F}}{dt} + 2\frac{d\mathcal{R}_\mathcal{F}}{dt}\frac{\delta\mathcal{R}_\mathcal{G}}{\delta t} + \frac{\delta\mathcal{R}_\mathcal{G}}{\delta t}\frac{\delta\mathcal{R}_\mathcal{G}}{\delta t} + 2\frac{\delta\mathcal{R}_\mathcal{G}}{\delta t}(\omega\times\mathcal{R}_\mathcal{G}) + (\omega\times\mathcal{R}_\mathcal{G})(\omega\times\mathcal{R}_\mathcal{G}) + 2(\omega\times\mathcal{R}_\mathcal{G})\frac{d\mathcal{R}_\mathcal{F}}{dt} \right\}\rho\,\mathrm{d}V \tag{2}$$

$$\mathcal{U} = -\int_V (\mathcal{R}_\mathcal{F} + \mathcal{R}_\mathcal{G})g\rho\,\mathrm{d}V - \frac{1}{2}\int_V \frac{\delta^2\mathcal{R}_\mathcal{G}}{\delta t^2}\mathcal{R}_\mathcal{G}\rho\,\mathrm{d}V \tag{3}$$

We can express the position of the mass element ρdV relative to the body frame $\mathcal{G}$ as

$$\mathcal{R}_\mathcal{G} = \bar{s} + w(\bar{x}, t) \tag{4}$$

Here, $\bar{s}$ is the constant undeformed length, $w(\bar{x}, t)$ is the relative elastic displacement, and $\bar{x}$ is the generalized coordinate on the body frame. Assuming that the free vibration modes of the elastic body are known, we can express the relative displacement $w(\bar{x}, t)$ in terms of an infinite number of mode shapes $W(\bar{x})$ and generalized displacement coordinates $\Upsilon(t)$ as

$$w(\bar{x}, t) = \sum_{j=1}^{\infty} W_j(\bar{x})\Upsilon_j(t) \tag{5}$$

Using Eq. (5) and applying the mean axes theorem [6,30–32], we can rewrite Eqs. (2) and (3) as

$$\mathcal{T} = \frac{1}{2}m\frac{d\mathcal{R}_\mathcal{F}}{dt}\frac{d\mathcal{R}_\mathcal{F}}{dt} + \frac{1}{2}\omega^T I\omega + \frac{1}{2}\sum_{j=1}^{\infty} M_j\dot{\Upsilon}_j^2(t) \tag{6}$$

$$\mathcal{U} = -mg\mathcal{R}_\mathcal{F} + \frac{1}{2}\sum_{j=1}^{\infty}\bar{\omega}_j^2 M_j\Upsilon_j^2(t) \tag{7}$$

where the first, second, and third terms in Eq. (6) are translational $\mathcal{T}_t$, rotational $\mathcal{T}_r$, and elastic $\mathcal{T}_e$ kinetic energy terms. On the other hand, the first and second terms (7) are gravitational $\mathcal{U}_g$ and elastic $\mathcal{U}_e$ potential energy terms. The term M_j is the generalized mass term, and $\bar{\omega}_j$ is the natural frequency corresponding to the jth elastic degree of freedom.

B. Equations of Motion for Elastic Quadrotor UAV

The elastic quadrotor UAV[‡] is composed of three types of masses: the main body mass m_b, arm mass m_c, and rotor mass m_r. The total mass of the UAV is given by $m = m_b + 4m_c + 4m_r$, as depicted in Fig. 2. The position vector and Euler angles vector for the center of mass in the body frame are denoted by $\xi = [x, y, z]^\top \in \mathbb{R}^3$ and $\upsilon = [\phi, \theta, \psi]^\top \in \mathbb{R}^3$, respectively. The angular velocity vector of the center of mass in the inertial frame is $\omega = [p, q, r]^\top \in \mathbb{R}^3$. The rotation matrix $R_B \in \mathbb{R}^{3\times3}$ that transforms the vectors from $\mathcal{G}$ to $\mathcal{F}$ is given as

[‡]© 2021 Institute of Electrical and Electronics Engineers. Reprinted and updated, with permission, from E. Eraslan and Y. Yildiz, "Modeling and Adaptive Control of Flexible Quadrotor UAVs," 60th IEEE Conference on Decision and Control, Institute of Electrical and Electronics Engineers, Austin, TX, 2021, pp. 1783-1788.

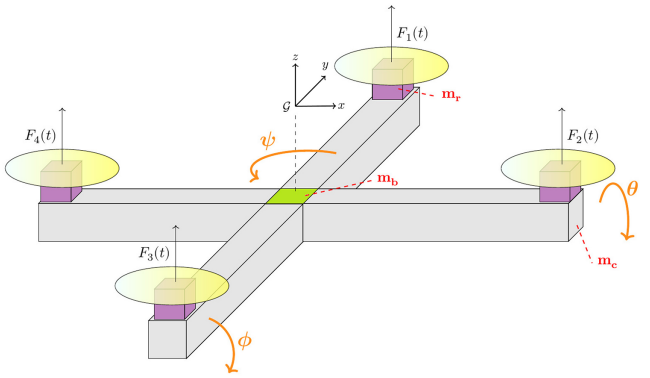

Fig. 2 A simplified schematic of the elastic quadrotor UAV. The body-fixed frame $\mathcal{G}$ is drawn slightly above the center of mass to prevent cluttering the illustration.

$$R_B = \begin{bmatrix} c_\psi c_\theta & c_\psi s_\theta s_\phi - s_\psi c_\phi & c_\psi s_\theta c_\phi + s_\psi s_\phi \\ s_\psi c_\theta & s_\psi s_\theta s_\phi + c_\psi c_\phi & s_\psi s_\theta c_\phi - c_\psi s_\phi \\ -s_\theta & c_\theta s_\phi & c_\theta c_\phi \end{bmatrix} \tag{8}$$

where s_υ and c_υ denote the sine and cosine of the corresponding Euler angle, respectively. The thrust force on the kth rotor is given by

$$F_k = k_t \Omega_k^2 \tag{9}$$

where k_t is the thrust factor and Ω_k is the angular velocity of the kth rotor. The total thrust force F_b represented in the body frame $\mathcal{G}$ is

$$F_b = \sum_{k=1}^{4} F_k \mathfrak{g}_3 \tag{10}$$

where $\mathfrak{g}_3 = [0, 0, 1]^\top$ is the unit vector that corresponds to the opposite direction of gravity in the body frame $\mathcal{G}$. F_b represented in the inertial frame $\mathcal{F}$ is given as

$$\mathcal{Q}_\xi = R_B F_b \tag{11}$$

The torques developed due to the rotational velocities of the rotors are calculated as

$$\tau_b = \begin{bmatrix} \tau_\phi \\ \tau_\theta \\ \tau_\psi \end{bmatrix} = \begin{bmatrix} k_t L_c (\Omega_4^2 - \Omega_2^2) \\ k_t L_c (\Omega_3^2 - \Omega_1^2) \\ k_q (-\Omega_1^2 + \Omega_2^2 - \Omega_3^2 + \Omega_4^2) \end{bmatrix} \tag{12}$$

where k_q is the drag factor and L_c is the arm length. Gyroscopic torques are given as

$$\begin{aligned} \tau_g &= -J_r \Omega_g [\dot{\upsilon} \times \mathfrak{g}_3], \\ \Omega_g &= \Omega_1 - \Omega_2 + \Omega_3 - \Omega_4 \end{aligned} \tag{13}$$

where J_r is the moment of inertia of the rotor and Ω_g is the gyroscopic velocity. The total torque $\mathcal{Q}_\upsilon$ represented in the inertial frame $\mathcal{F}$ is obtained as

$$\mathcal{Q}_\upsilon = \tau_b + \tau_g \tag{14}$$

The control input vector u is taken as

$$\begin{aligned} u &= \begin{bmatrix} k_t & k_t & k_t & k_t \\ 0 & -k_t & 0 & k_t \\ -k_t & 0 & k_t & 0 \\ -k_q & k_q & -k_q & k_q \end{bmatrix} \begin{bmatrix} \Omega_1^2 \\ \Omega_2^2 \\ \Omega_3^2 \\ \Omega_4^2 \end{bmatrix}, \\ &= R_{\Omega_s} \Omega_s \end{aligned} \tag{15}$$

where R_{Ω_s} is the corresponding constant transformation matrix and $\Omega_s = [\Omega_1^2, \Omega_2^2, \Omega_3^2, \Omega_4^2]^\top$ is the vector consisting of the squares of rotational velocities. Another useful transformation matrix is the one that converts the force vector $F = [F_1, F_2, F_3, F_4]^\top$ into the control input vector u. Multiplying Ω_s with k_t and dividing each element of R_{Ω_s} by k_t, it follows from Eq. (15) that

$$\begin{aligned} u &= k_t^{-1} R_{\Omega_s} F, \\ &= R_F F \end{aligned} \tag{16}$$

where R_F is the corresponding constant transformation matrix. The generalized coordinates for the elastic body dynamics is given as $q = [\xi^\top, \upsilon^\top, \Upsilon_j^\top]^\top \in \mathbb{R}^{(p+6)}$, $j = 1, 2, \ldots, p$, where p is the number of elastic degrees of freedom, which is infinite in theory but can be truncated to a finite number depending on the level of modeling fidelity. In this work, we set $p = 3$, that is, we take the first three natural frequency values of the quadrotor arms for the elastic body formulation. The relation between the rotational velocity vector ω and time rate of change of the Euler angles vector are expressed as

$$\begin{aligned} \omega &= \begin{bmatrix} -s_\theta & 0 & 1 \\ c_\theta s_\psi & c_\psi & 0 \\ c_\theta c_\psi & -s_\psi & 0 \end{bmatrix} \dot{\upsilon}, \\ &= R_\upsilon \dot{\upsilon} \end{aligned} \tag{17}$$

where R_υ is the corresponding transformation matrix. Substituting Eq. (17) into Eq. (6), it follows that

$$\mathcal{T}(q, \dot{q}) = \frac{1}{2} m \frac{d\mathcal{R}_\mathcal{F} d\mathcal{R}_\mathcal{F}}{dt \quad dt} + \frac{1}{2} \dot{\upsilon}^\top R^{\upsilon^\top} I R^\upsilon \dot{\upsilon} + \frac{1}{2} \sum_{j=1}^{\infty} M_j \dot{\Upsilon}_j^2(t) \tag{18}$$

The Lagrangian consisting of the set of generalized coordinates for the elastic quadrotor UAV can be expressed as

$$\mathcal{L}(q, \dot{q}) = \mathcal{T} - \mathcal{U} \tag{19}$$

The friction term is added exogenously to the formulation in terms of a Rayleigh dissipation function [27] as

$$\mathcal{D}(\dot{q}) = \frac{1}{2} \sum_{j=1}^{\infty} \sigma_c \dot{\Upsilon}_j^2(t) \tag{20}$$

where the term σ_c is the damping coefficient term. The Lagrangian equation is then given as

$$\frac{d}{dt}\left(\frac{\partial \mathcal{L}}{\partial \dot{q}_i}\right) - \left(\frac{\partial \mathcal{L}}{\partial q_i}\right) + \left(\frac{\partial \mathcal{D}}{\partial \dot{q}_i}\right) = \mathcal{Q}_i \tag{21}$$

where $i = 1, 2, \ldots, (p + 6)$ and Q_i is the generalized force. Using Eqs. (18–21), we obtain that

$$\ddot{x} = (c_\psi s_\theta c_\phi + s_\psi s_\phi) \frac{u_1}{m} \tag{22}$$

$$\ddot{y} = (s_\psi s_\theta c_\phi - c_\psi s_\phi) \frac{u_1}{m} \tag{23}$$

$$\ddot{z} = -g + (c_\theta c_\phi) \frac{u_1}{m} \tag{24}$$

$$\ddot{\phi} = \left(\frac{J_y - J_z}{J_x}\right) \dot{\theta}\dot{\psi} - \frac{J_r}{J_x} \Omega_g \dot{\theta} + \frac{L_c}{J_x} u_2 \tag{25}$$

$$\ddot{\theta} = \left(\frac{J_z - J_x}{J_y}\right) \dot{\phi}\dot{\psi} + \frac{J_r}{J_y} \Omega_g \dot{\phi} + \frac{L_c}{J_y} u_3 \tag{26}$$

$$\ddot{\psi} = \left(\frac{J_x - J_y}{J_z}\right)\dot{\phi}\dot{\theta} + \frac{1}{J_z}u_4 \tag{27}$$

$$M_j\ddot{\Upsilon}_j(t) + \sigma_c\dot{\Upsilon}_j(t) + \bar{\omega}_j^2 M_j\Upsilon_j(t) = \mathcal{Q}_{\Upsilon_j}(t) \tag{28}$$

Remark 1: The equations of motion comprise a rigid part (22–27) and an elastic part (28). The latter has a form similar to that of a p-many mass spring damper systems, where p is the number of elastic modes.

C. Transverse Vibrations of Elastic Arms

The equations of motion (see footnote 1)[§] governing the elastic part in Eq. (28) are relatively simple, but the meanings of terms like M_j, σ_c, $\bar{\omega}_j$, and $\mathcal{Q}_{\Upsilon_j}(t)$ in the overall system are unclear. If we consider the flexibility of the quadrotor, we can interpret the arms as thin cantilever beams undergoing transverse vibrations due to the continuous motion and agile maneuvers of the quadrotor (see Fig. 3).

While much research exists on the modeling of undamped Euler–Bernoulli beams under different boundary conditions, there are relatively few studies on beams with damping. One approach involves using the viscoelastic Kelvin–Voigt model as an internal property, as done by [33,34]. Another approach is to attach a dash pot at the free end of a cantilever beam to create external damping, as in the models developed by [35,36]. For simplicity, we use the latter approach and write the equations of motion for the damped beam shown in Fig. 3 as

$$E_cJ_c\frac{\partial^4 w(\bar{x},t)}{\partial\bar{x}^4} + \rho_cA_c\frac{\partial^2 w(\bar{x},t)}{\partial t^2} + \sigma_c\frac{\partial w(\bar{x},t)}{\partial t} = F(\bar{x},t) \tag{29}$$

where E_c and J_c are the Young's modulus and moment of inertia of the beam, respectively; ρ_c is the density; A_c is the cross-sectional area; σ_c is the damping coefficient of the beam; and $F(\bar{x},t)$ is the concentrated thrust force acting at the beam edge. The solution to the homogeneous part of this equation can be obtained by using Eq. (5), which consists of the mode shape $W_j(\bar{x})$ and the generalized displacement coordinates $\Upsilon_j(t)$. Because the beam is fixed to the moving main rigid body m_b at one end and carries the rotor mass m_r at the other end, the boundary conditions can be stated as

$$W(0) = 0 \tag{30}$$

$$\frac{dW(0)}{d\bar{x}} = 0 \tag{31}$$

$$E_cJ_c\frac{d^2W(L_c)}{d^2\bar{x}} = 0 \tag{32}$$

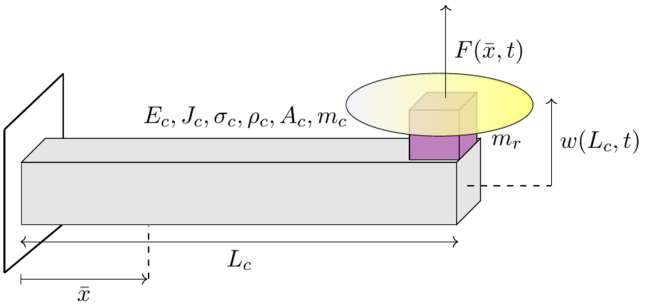

Fig. 3 An illustration of the elastic quadrotor arm as a cantilever carrying a rotor.

$$E_cJ_c\frac{\partial^3 w(L_c,t)}{\partial^3\bar{x}} = m_r\frac{\partial^2 w(L_c,t)}{\partial^2 t} \tag{33}$$

Taking $F(\bar{x},t) = 0$, substituting Eq. (5) into Eq. (29), and solving it together with Eqs. (30–33), the transcendental frequency equation [37] is obtained as

$$1 + \frac{1}{\cos\bar{\beta}_j\cosh\bar{\beta}_j} - \bar{m}\bar{\beta}_j(\tan\bar{\beta}_j - \tanh\bar{\beta}_j) = 0 \tag{34}$$

$$\beta_j = \sqrt[4]{\frac{\rho_cA_c\bar{\omega}_j^2}{E_cJ_c}} \tag{35}$$

where $\bar{\beta}_j = \beta_jL_c$ is the solution of Eq. (34), β_j is a specific constant obtained from the separation of Eq. (29) corresponding to the jth natural frequency $\bar{\omega}_j$, and $\bar{m} = m_r/m_c$ denotes the ratio of the rotor mass m_r to the mass of the cantilever beam m_c. For a given jth mode, we can solve for $\bar{\beta}_j$ in Eq. (34) and calculate a corresponding natural frequency $\bar{\omega}_j$ in Eq. (35). Following this procedure, we also obtain the mode shape $W_j(\bar{x})$, which can be written as

$$W_j(\bar{x}) = \bar{\gamma}_j \times\left[(\cos\beta_j\bar{x} - \cosh\beta_j\bar{x}) - \frac{\cos\bar{\beta}_j + \cosh\bar{\beta}_j}{\sin\bar{\beta}_j + \sinh\bar{\beta}_j}(\sin\beta_j\bar{x} - \sinh\beta_j\bar{x})\right] \tag{36}$$

where $\bar{\gamma}_j$ is a normalization constant corresponding to the jth mode (see Appendix A). Having found the mode shapes $W_j(\bar{x})$ in Eq. (5), it remains to find the solutions of the generalized displacement coordinates $\Upsilon_j(t)$ in Eq. (28). Applying orthogonality conditions (see Appendix B), it is obtained that

$$\ddot{\Upsilon}_j(t) + \sigma_c'\dot{\Upsilon}_j(t) + \bar{\omega}_j^2\Upsilon_j(t) = \int_0^{L_c} W_j(\bar{x})F(\bar{x},t)\,\mathrm{d}\bar{x} \tag{37}$$

where $\sigma_c' = \sigma_c/(\rho_cA_c)$. It is noted that there is a one-to-one correspondence between Eqs. (28) and (37). The generalized mass term M_j in Eq. (28) refers to ρ_cA_c, which is the mass per unit length. Considering the right-hand side of Eq. (37) and recalling that $F_k(\bar{x},t) = F_k(t)\delta(\bar{x} - L_c)$ is a concentrated thrust force for the kth quadrotor arm, $k = \{1,2,3,4\}$, where $\delta(\bar{x})$ is the Dirac's delta function, it can be shown that

$$\int_0^{L_c} W_j(\bar{x})F_k(t)\delta(\bar{x} - L_c)\,\mathrm{d}\bar{x} = W_j(L_c)F_k(t) \tag{38}$$

Substituting Eq. (38) into Eq. (37), we obtain that

$$\ddot{\Upsilon}_{kj}(t) + \sigma_c'\dot{\Upsilon}_{kj}(t) + \bar{\omega}_{kj}^2\Upsilon_{kj}(t) = W_j(L_c)F_k(t), \quad j = 1,2,\ldots,\infty \tag{39}$$

For each arm of the quadrotor, Eq. (39) has infinitely many solutions corresponding to each $\bar{\omega}_j$. We choose to take the first three natural frequency values; that is, the variable j takes the values of 1, 2, and 3. The relative displacement $w_k(\bar{x},t)$ of the arm k at the tip can then be calculated as

$$w_k(L_c,t) = \sum_{j=1}^{3} W_j(L_c)\Upsilon_{kj}(t) \tag{40}$$

Using Eq. (40), we define the corresponding elastic states z_{kj}, with $k = \{1,2,3,4\}$ and $j = \{1,2,3\}$, as

$$z_{kj}(t) = W_j(L_c)\Upsilon_{kj}(t) \tag{41}$$

[§]© 2021 Institute of Electrical and Electronics Engineers. Reprinted, with permission, from E. Eraslan and Y. Yildiz, "Modeling and Adaptive Control of Flexible Quadrotor UAVs," 2021 60th IEEE Conference on Decision and Control (CDC), Austin, TX, USA, 2021, pp. 1783-1788.

Multiplying Eq. (39) with $W_j(L_c)$ and using Eq. (41), Eq. (39) can be rewritten as

$$\ddot{z}_{kj}(t) + \sigma_c'\dot{z}_{kj}(t) + \bar{\omega}_{kj}^2 z_{kj}(t) = W_j^2(L_c)F_k(t) \tag{42}$$

This implies that the tip oscillations at each arm k can be modeled as the summation of solutions of three mass spring damper systems with the same damping coefficient σ_c' but different spring constants $\bar{\omega}_{kj}^2$. Therefore, the elastic states for arm k can be written in a state space form as

$$\dot{z}_e^k = A_e' z_e^k + B_{ze}' F_k \tag{43}$$

where $z_e^k = [z_{k1}, \dot{z}_{k1}, z_{k2}, \dot{z}_{k2}, z_{k3}, \dot{z}_{k3}]^\top$, and

$$A_e' = \begin{bmatrix} 0 & 1 & 0 & 0 & 0 & 0 \\ -\bar{\omega}_1^2 & -\sigma_c' & 0 & 0 & 0 & 0 \\ 0 & 0 & 0 & 1 & 0 & 0 \\ 0 & 0 & -\bar{\omega}_2^2 & -\sigma_c' & 0 & 0 \\ 0 & 0 & 0 & 0 & 0 & 1 \\ 0 & 0 & 0 & 0 & -\bar{\omega}_3^2 & -\sigma_c' \end{bmatrix}, \quad B_{ze}' = \begin{bmatrix} 0 \\ W_1^2(L_c) \\ 0 \\ W_2^2(L_c) \\ 0 \\ W_3^2(L_c) \end{bmatrix} \tag{44}$$

Finally, the whole elastic state space formulation can be constructed as

$$\dot{z}_e = A_e z_e + B_{ze} F \tag{45}$$

where $F = [F_1, F_2, F_3, F_4]^\top$, and

$$A_e = \begin{bmatrix} A_e' & 0_{6\times6} & 0_{6\times6} & 0_{6\times6} \\ 0_{6\times6} & A_e' & 0_{6\times6} & 0_{6\times6} \\ 0_{6\times6} & 0_{6\times6} & A_e' & 0_{6\times6} \\ 0_{6\times6} & 0_{6\times6} & 0_{6\times6} & A_e' \end{bmatrix}, \quad B_{ze} = \begin{bmatrix} B_{ze}' & 0_{6\times1} & 0_{6\times1} & 0_{6\times1} \\ 0_{6\times1} & B_{ze}' & 0_{6\times1} & 0_{6\times1} \\ 0_{6\times1} & 0_{6\times1} & B_{ze}' & 0_{6\times1} \\ 0_{6\times1} & 0_{6\times1} & 0_{6\times1} & B_{ze}' \end{bmatrix} \tag{46}$$

Using Eq. (16), the thrust vector can be written in terms of the control input vector u as $F = R_F^{-1}u$. Substituting this into Eq. (45), defining $B_e = B_{ze}R_F^{-1}$, and introducing an actuator effectiveness matrix Λ, it is obtained that

$$\dot{z}_e = A_e z_e + B_e \Lambda u \tag{47}$$

Remark 2: Because the matrix A_e is stable, the subsystem (47) is bounded-input bounded-states stable. Although this stability result enables a controller design that is based on rigid-body dynamics, the designer needs to ensure that control input excitations are not close to the natural frequencies of the elastic modes, and arm tip oscillations are minimized. We discuss these issues in Sec. III.

III. Controller Design

The overall closed-loop control system can be analyzed in two parts, namely, an outer loop and an inner loop. This loop constitutes the uncertain elastic quadrotor dynamics with a DRCRM adaptive controller (see Fig. 4). The human operator exists in the outer loop, where s/he observes the commanded and actual plant states, and produces a reference input for the inner loop. In the following, we first explain the DRCRM adaptive controller design for two cases: 1) autonomous flight with a predefined reference input and 2) an operator controlled flight with a reference input changing in real time. Then, we provide an overall stability analysis in the presence of the human operator.

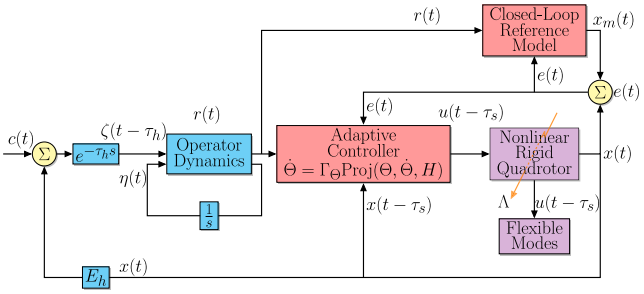

Fig. 4 Block diagram of the overall control architecture with an operator delay τ_h and input delay τ_s. The term $x(t-\tau_s)$ refers to delayed feedback. ©[2021] Institute of Electrical and Electronics Engineers. Reprinted and updated, with permission, from E. Eraslan and Y. Yildiz, "Modeling and Adaptive Control of Flexible Quadrotor UAVs," 60th IEEE Conference on Decision and Control (CDC), Institute of Electrical and Electronics Engineers, Austin, TX, 2021, pp. 1783-1788.

A. DRCRM Controller for Predefined Reference Input $r(t)$

Linearizing the equations of motion in Eqs. (22–27) by using small angle approximations, we obtain that

$$\begin{aligned} \dot{x}_p(t) &= A_p x_p(t) + B_p \Lambda u(t-\tau_s) \\ y_p(t) &= C_p x_p(t) \end{aligned} \tag{48}$$

where $x_p \in \mathbb{R}^{n_p}$ comprises the position and the Euler angles variables and their corresponding derivatives, $u \in \mathbb{R}^{n_m}$ is the control input, τ_s is the input delay, and $y_p \in \mathbb{R}^{n_r}$ is the plant output. Besides, $A_p \in \mathbb{R}^{n_p\times n_p}$ is constant and unknown; $B_p \in \mathbb{R}^{n_p\times n_m}$ is a known constant matrix, with the assumption that (A_p, B_p) is controllable; and $\Lambda \in \mathbb{R}^{n_m\times n_m}$ is an unknown positive definite matrix representing the control effectiveness. The evolution of the elastic states is given in Eq. (47). The control goal of interest is bounded command tracking in the presence of uncertainties, that is, tracking a reference $r(t) \in \mathbb{R}^{n_r}$. To achieve tracking, a new state vector $e_p \in \mathbb{R}^{n_r}$ is defined as the integral of the tracking error,

$$e_p(t) = \int_0^t [y_p(\varepsilon) - r(\varepsilon)]\,\mathrm{d}\varepsilon \tag{49}$$

and augmented with Eq. (48), which results in the dynamics

$$\dot{x}(t) = Ax(t) + B\Lambda u(t-\tau_s) + B_m r(t) \tag{50}$$

where

$$A = \begin{bmatrix} A_p & 0_{n_p\times n_m} \\ C_p & 0_{n_m\times n_m} \end{bmatrix}, \quad B = \begin{bmatrix} B_p \\ 0_{n_m\times n_m} \end{bmatrix}, \quad B_m = \begin{bmatrix} 0_{n_p\times n_r} \\ -I_{n_r\times n_r} \end{bmatrix} \tag{51}$$

and $x(t) = [x_p(t)^T, e_p(t)^T]^T \in \mathbb{R}^{(n_p+n_m)}$ is the augmented state vector with $n = n_p + n_m$. The goal is to stabilize the plant and track the output of a stable reference model. Assuming that there exists a K_d^* such that $A - B\Lambda K_d^* = A_m$, where A_m is a stable matrix, substituting the control input

$$u(t) = -K_d^* x(t+\tau_s) \tag{52}$$

into Eq. (50), we obtain that

$$\dot{x}(t) = A_m x(t) + B_m r(t) \tag{53}$$

Although the controller given in Eq. (52) is noncausal, it can be expressed in a causal form by analytically solving Eq. (50) as

$$x(t+\tau_s) = e^{A\tau_s}x(t) + \int_{-\tau_s}^{0} e^{-A\eta}B\Lambda u(t+\eta)\,\mathrm{d}\eta + \int_{-\tau_s}^{0} e^{-A\eta}B_m r(t+\tau_s+\eta)\,\mathrm{d}\eta \tag{54}$$

Because K_d^* is unknown, we use a control input of the form

$$u(t) = -K_d(t)x(t+\tau_s) \tag{55}$$

and with the help of Eq. (54), we obtain that

$$u(t) = -K_d(t)\left[e^{A\tau_s}x(t) + \int_{-\tau_s}^{0} e^{-A\eta}B\Lambda u(t+\eta)\,\mathrm{d}\eta + \int_{-\tau_s}^{0} e^{-A\eta}B_m r(t+\tau_s+\eta)\,\mathrm{d}\eta\right] \tag{56}$$

By defining $K_x(t) = K_d(t)e^{A\tau_s}$, $\lambda_u(t,\eta) = K_d(t)e^{-A\eta}B\Lambda$, and $\lambda_r(t,\eta) = K_d(t)e^{-A\eta}B_m$, we rewrite Eq. (56) as

$$u(t) = -K_x(t)x(t) - \int_{-\tau_s}^{0} \lambda_u(t,\eta)u(t+\eta)\,\mathrm{d}\eta - \int_{-\tau_s}^{0} \lambda_r(t,\eta)r(t+\tau_s+\eta)\,\mathrm{d}\eta \tag{57}$$

where the corresponding ideal values for the adaptive parameters are $K_x^* = K_d^*e^{A\tau_s}$, $\lambda_u^*(\eta) = K_d^*e^{-A\eta}B\Lambda$, and $\lambda_r^*(\eta) = K_d^*e^{-A\eta}B_m$. Substituting Eq. (57) into Eq. (50), we obtain that

$$\dot{x}(t) = A_m x(t) - B\Lambda[\tilde{K}_x(t-\tau_s)x(t-\tau_s) + \int_{-\tau_s}^{0} \tilde{\lambda}_u(t-\tau_s,\eta)u(t-\tau_s+\eta)\,\mathrm{d}\eta + \int_{-\tau_s}^{0} \tilde{\lambda}_r(t-\tau_s,\eta)r(t+\eta)\,\mathrm{d}\eta] + B_m r(t-\tau_s) \tag{58}$$

where $\tilde{K}_x(t) = K_x(t) - K_x^*$, $\tilde{\lambda}_u(t,\eta) = \lambda_u(t,\eta) - \lambda_u^*(\eta)$, and $\tilde{\lambda}_r(t,\eta) = \lambda_r(t,\eta) - \lambda_r^*(\eta)$. Defining a reference model as

$$\dot{x}_m(t) = A_m x_m(t) + B_m r(t-\tau_s) - Le(t) \tag{59}$$

where $e = x - x_m$, the error dynamics can be obtained by subtracting Eq. (59) from Eq. (58) as

$$\dot{e}(t) = A_m e(t) - B\Lambda[\tilde{K}_x(t-\tau_s)x(t-\tau_s) + \int_{-\tau_s}^{0} \tilde{\lambda}_u(t-\tau_s,\eta)u(t-\tau_s+\eta)\,\mathrm{d}\eta + \int_{-\tau_s}^{0} \tilde{\lambda}_r(t-\tau_s,\eta)r(t+\eta)\,\mathrm{d}\eta] + Le(t) \tag{60}$$

The control parameters are updated using the adaptive laws

$$\dot{K}_x^{\top}(t) = -\Gamma_x x(t-\tau_s)e(t)^{\top}PB \tag{61}$$

$$\dot{\lambda}_u^{\top}(t,\eta) = -\Gamma_{\lambda_u} u(t-\tau_s+\eta)e(t)^{\top}PB \tag{62}$$

$$\dot{\lambda}_r^{\top}(t,\eta) = -\Gamma_{\lambda_r} r(t+\eta)e(t)^{\top}PB \tag{63}$$

where $\Gamma_x \in \mathbb{R}^{n\times n}$, $\Gamma_{\lambda_u} \in \mathbb{R}^{n\times n_m}$, and $\Gamma_{\lambda_r} \in \mathbb{R}^{n\times n_r}$ are diagonal positive definite matrices of adaptive gains and $P \in \mathbb{R}^{n\times n}$ is the unique symmetric positive definite solution of the Lyapunov equation $(A_m + L)^{\top}P + P(A_m + L) = -Q$, where $Q \in \mathbb{R}^{n\times n} > 0$ is a positive definite symmetric matrix.

Remark 3: Because in this section we are considering a predefined reference signal, $r(t+\eta)$ required in Eq. (63) is available.

To prevent adaptive parameter drifts, we use the projection algorithm [38] as

$$\dot{\hat{K}}_x^{\top}(t) = -\Gamma_x \mathrm{Proj}(\hat{K}_x^{\top}(t), x(t-\tau_s)e(t)^{\top}PB, H) \tag{64}$$

$$\dot{\hat{\lambda}}_u^{\top}(t,\eta) = -\Gamma_{\lambda_u} \mathrm{Proj}(\hat{\lambda}_u^{\top}(t), u(t-\tau_s+\eta)e(t)^{\top}PB, H) \tag{65}$$

$$\dot{\hat{\lambda}}_r^{\top}(t,\eta) = -\Gamma_{\lambda_r} \mathrm{Proj}(\hat{\lambda}_r^{\top}(t), r(t+\eta)e(t)^{\top}PB, H) \tag{66}$$

where the projection operator is defined as

$$\mathrm{Proj}(\Theta, Y, H) = [\mathrm{Proj}(\theta_1, y_1, h_1)\ldots\mathrm{Proj}(\theta_m, y_m, h_m)] \tag{67}$$

where $\Theta = [\theta_1\ldots\theta_m] \in \mathbb{R}^{(n_s+n)\times n_m}$, $Y = [y_1\ \ldots\ y_m] \in \mathbb{R}^{(n_s+n)\times n_m}$, and $H = [h_1(\theta_1)\ldots h_m(\theta_m)]^{\top} \in \mathbb{R}^{n_m\times 1}$. The vector form of the projection operator is

$$\mathrm{Proj}(\theta_j, y_j, h_j) = \begin{cases} y_j - \frac{\nabla h_j(\theta_j)(\nabla h_j(\theta_j))^{\top}}{\left\|\nabla h_j(\theta_j)\right\|^2} y_j h_j(\theta_j) & \text{if } h_j(\theta_j) > 0 \wedge y_j^{\top}\nabla h_j(\theta_j) > 0 \\ y_j & \text{otherwise} \end{cases} \tag{68}$$

where $h : \mathbb{R}^{n_m} \to \mathbb{R}$ is a convex function and $\nabla h(\theta) = \left(\frac{\partial h(\theta)}{\partial \theta_1}\cdots\frac{\partial h(\theta)}{\partial \theta_{n_m}}\right)^{\top}$. Considering the error dynamics (60) and the adaptive control laws (64–66), it can be shown that the DRCRM controller for a predefined reference input has bounded solutions for all $t \geq 0$. Furthermore, if the reference model (59) is bounded, then it can be shown that the tracking error e in Eq. (60) converges to 0. The boundedness of the reference model is proven in the Sec. III.C. Assuming that the reference model is bounded, we express the stability result of the DRCRM controller precisely in Theorem III.1. It is noted that, once the tracking error is derived in a form given in Eq. (60), the proof of Theorem III.1 follows a similar logic given in [39], in which a simpler error dynamics without an integral state is used. Therefore, we omit the proof of this theorem for brevity.

Theorem III.1: Given the initial conditions $\tilde{K}_x(\vartheta)$, $\tilde{\lambda}_u(\vartheta,\eta)$, $\tilde{\lambda}_r(\vartheta,\eta)$ and $x(\vartheta)$ for $\vartheta \in [-\tau_s, 0]$ and $u(\varrho)$ for $\varrho \in [-2\tau_s, 0]$, there exists a τ_s^* such that for all $\tau_s \in [0, \tau_s^*]$ the closed-loop system with the DRCRM controller, described by Eqs. (50), (57), and (64–66), has bounded solutions for all $t \geq 0$, and $\lim_{t\to\infty} e(t) = 0$.

B. DRCRM Controller for Real-Time Operator Control

For systems with time delay, the method of integrating the tracking error is not a feasible way to solve the adaptive control problem if the quadrotor UAV is controlled in real time by an operator; in other words, if the future of the reference $r(t)$ cannot be known beforehand (see Remark 3). Consider the nominal plant dynamics

$$\dot{x}_n(t) = A_n x_n(t) + B_p u(t-\tau_s)$$
$$y_n(t) = C_p^{\top} x_n(t) \tag{69}$$

Implementing the nominal control input

$$u_n(t) = -\varphi_\alpha^{\top} x_n(t+\tau_s) + \varphi_\beta^{\top} r(t) \tag{70}$$

leads to a closed-loop system of the form

$$\dot{x}_n(t) = A_m x_n(t) + B_p\varphi_\beta^{\top} r(t-\tau_s)$$
$$y_n(t) = C_p^{\top} x_n(t) \tag{71}$$

where $A_m = A_n - B_p\varphi_\alpha^{\top}$. Choosing a $\varphi_\alpha^{\top}$ linear-quadratic regulator (LQR) gain such that A_m is Hurwitz, we obtain that

$$y_n(t) = C_p^\top (sI - A_m)^{-1} B_p \varphi_\beta^\top r(t - \tau_s) \tag{72}$$

For a constant r, it is observed that

$$y_n(t) = -C_p^\top A_m^{-1} B_p \varphi_\beta^\top r \tag{73}$$

Selecting $\varphi_\beta^\top = -(C_p^\top A_m^{-1} B_p)^{-1}$ results in $\lim_{t\to\infty}(y_p(t) - r(t)) = 0$. Then, using the reference model, where state and input matrices are selected as A_m and $B_p\varphi_\beta$, a similar procedure given in [40] can be implemented to design the adaptive controller. It is noted that Eq. (70) is not causal as analogous to the case given in Eq. (52). Following the same approach, the nominal control input can be obtained in a similar form to that of Eq. (56) as

$$u_n(t) = -\varphi_\alpha^\top \left[e^{A_n \tau_s} x(t) + \int_{-\tau_s}^{0} e^{-A_n \eta} B_p u(t+\eta)\, \mathrm{d}\eta \right] + \varphi_\beta^\top r(t) \tag{74}$$

Considering the uncertain plant dynamics with input delay τ_s (48) and the closed-loop reference model (59), an adaptive control input u_{ad}, which has a similar form to that of Eq. (57) except the integral term, can be added to the nominal controller such that the overall control input for DRCRM becomes

$$u(t) = u_n(t) + u_{\mathrm{ad}}(t) \tag{75}$$

where

$$u_{\mathrm{ad}}(t) = \varphi_x^\top(t) x_p(t) + \int_{-\tau_s}^{0} \varphi_\lambda(t,\eta) u(t+\eta)\, \mathrm{d}\eta + \varphi_r^\top(t) r(t) \tag{76}$$

with the assumption that ideal DRCRM controller parameters exist such that $A_m = A_p - B_n \Lambda \varphi_\alpha^{*\top}$ and $\varphi_r^{*\top} = \Lambda^{-1}\varphi_\beta$. The control parameters together with the aforementioned projection algorithm are given as

$$\dot{\varphi}_x(t) = -\Gamma_{\varphi_x} \mathrm{Proj}(\hat{\varphi}_x^\top(t), x_p(t-\tau_s) e(t)^\top P B_n, H) \tag{77}$$

$$\dot{\varphi}_\lambda(t,\eta) = -\Gamma_{\varphi_\lambda} \mathrm{Proj}(\hat{\varphi}_\lambda^\top(t), u(t-\tau_s+\eta) e(t)^\top P B_n, H) \tag{78}$$

$$\dot{\varphi}_r(t,\eta) = -\Gamma_{\varphi_r} \mathrm{Proj}(\hat{\varphi}_r^\top(t), r(t-\tau_s) e(t)^\top P B_n, H) \tag{79}$$

where Γ_{φ_x}, Γ_{φ_λ}, and Γ_{φ_r} are the corresponding adaptation gains. Then, using Theorem III.1, the DRCRM controller for real-time reference signal can be shown to have bounded solutions for all $t \geq 0$, and the tracking error converges to 0. It is noted that the convergence of the tracking error to 0 hinges upon the assumption that the reference model is bounded, which has not been validated yet. The boundedness of the reference model together with the human operator having a reaction time delay is investigated in the next section.

C. Outer-Loop Dynamics

Pilot models have different utility depending on the specific application. For instance, a constant gain model is suitable for investigating pilot-induced oscillations [41], and a gain and a low-pass-filter model are used to represent the frequency limited response of humans [42–44]. In this section, we follow the steps similar to those given in [45] to analyze overall closed-loop system stability and employ a linear model with time delay for human operator dynamics that is general enough to capture the Neal–Smith criteria and its extensions [46–48]. The pilot model dynamics is represented as

$$\dot{\eta}(t) = A_h \eta(t) + B_h \zeta(t - \tau_h) \tag{80}$$

$$r(t) = C_h \eta(t) + D_h \zeta(t - \tau_h) \tag{81}$$

where $\eta(t) \in \mathbb{R}^{n_\eta}$ is the human state vector; $\tau_h \in \mathbb{R}^+$ is the reaction delay; and $A_h \in \mathbb{R}^{n_\eta \times n_\eta}$, $B_h \in \mathbb{R}^{n_\eta \times n_c}$, $C_h \in \mathbb{R}^{n_r \times n_\eta}$ and $D_h \in \mathbb{R}^{n_r \times n_c}$ are constant matrices. The reference formed by the human operator is $r(t) \in \mathbb{R}^{n_r}$. The input to the human dynamics is the feedback error term

$$\zeta(t) = c(t) - E_h x(t) \tag{82}$$

where $E_h \in \mathbb{R}^{n_c \times n}$ is a constant matrix that allows to choose a subset of the state $x(t)$, given in Eq. (58), as feedback. Using Eqs. (81) and (82), Eqs. (59) and (80) can be rewritten compactly as a single delay equation as

$$\dot{\mu}(t) = \mathcal{A}_n \mu(t) + \mathcal{A}_d \mu(t - \tau_h) + \Pi(\cdot) \tag{83}$$

where $\mu_h(t) \triangleq [x_m^\top(t), \eta^\top(t)]^\top$, and

$$\mathcal{A}_n = \begin{bmatrix} A_m & B_m C_h \\ 0_{n_\eta \times n} & A_h \end{bmatrix}, \quad \mathcal{A}_d = \begin{bmatrix} -B_m D_h E_h & 0_{n \times n_\eta} \\ -B_h E_h & 0_{n_\eta \times n_\eta} \end{bmatrix},$$
$$\Pi(\cdot) = \begin{bmatrix} -Le(t) - B_m D_h E_h e(t-\tau_h) + B_m D_h c(t-\tau_h) \\ -B_h E_h e(t-\tau_h) + B_h c(t-\tau_h) \end{bmatrix} \tag{84}$$

Because it is shown that the tracking error $e(t)$ is bounded in the previous sections and the command $c(t)$ is bounded, $\Pi(\cdot)$ is also bounded.

Theorem III.2: Consider the dynamics given in Eq. (83). If the real parts of all the infinitely many roots of the equation

$$\det\left(sI - (\mathcal{A}_n + \mathcal{A}_d e^{-\tau_h s})\right) = 0 \tag{85}$$

have strictly negative real parts, then $\mu_h(t) \in \mathcal{L}_\infty$.

Proof 1: If all of the roots of the characteristic equation (85) have strictly negative real parts, then the homogeneous part of Eq. (83), given as

$$\dot{\mu}_h(t) = \mathcal{A}_n \mu_h(t) + \mathcal{A}_d \mu_h(t - \tau_h) \tag{86}$$

is stable. Furthermore, because the forcing term $\Pi(\cdot)$ in Eq. (83) is bounded, the solution $\mu(t)$ is bounded. This implies that both the reference model state $x_m(t)$ and the human state $\eta(t)$ are bounded. □

Remark 4: The stability analysis of the inner loop is completed in the previous sections. The boundedness of all system signals are shown, and it is stated that for the state tracking error to converge to 0 the reference model needs to be bounded. In this section, we prove the boundedness of the reference model. Therefore, the stability analysis of the overall closed-loop system is completed.

Remark 5: Theorem III.2 is proved assuming that the inner-loop controller, DRCRM, receives a predefined reference input (see Sec. III.A). The proof for the case where the reference is not predefined (see Sec. III.B) follows the same steps as the previous case and is therefore omitted for brevity.

Remark 6: Depending on the application, stability limits of the overall system change based on the roots of Eq. (85). In the following section, we demonstrate this change for our simulation example.

IV. Simulations

In this section, a number of simulations are performed in order to demonstrate the stability and performance characteristics of the human-in-the-loop control system, consisting of the human operator, the controller, and the flexible UAV, in the presence of quadrotor input delay and human reaction delay. In the following, we first explain the simulation scenario, the controller design details, and the stability limits of the operator dynamics and then discuss the simulation results.

A. Simulation Scenario

In the simulations, the elastic UAV equations of motion introduced in Eqs. (22–27) and (47) are used as the plant model. The human operator model is represented as

$$G_{\mathrm{PI}}(s) = K_p \frac{T_p s + 1}{s} e^{-\tau_h s} \tag{87}$$

where $K_p > 0$ and $T_p > 0$ are model constants and τ_h is the human operator reaction time delay. This model is consistent with Eqs. (80–82) and with lead/lag-type pilot models used in closed-loop flight control system analysis [46–48].

An operator controlled flight condition is simulated: the human operator's goal is to make the UAV follow a desired altitude command z_d, by producing a corresponding reference input, which is fed to the controller (see Fig. 4). During this simulation, the rest of the position and attitude references which are x_d, y_d, and ψ_d are created externally. In a simulation of 70 s, two anomalies are injected at $t_a = 16$ s, which result in loss of control effectiveness of 75% and 50% in the second and third rotors, respectively.

B. Controller Design Details

The baseline controller gain vectors ϕ_α and ϕ_β in Eq. (70) are first calculated based on the nominal plant dynamics. Then, the elements of this vector is decreased by 20% to introduce additional uncertainty. For the design of the adaptive controller, three sets of design parameters need to be determined: adaptation rates, initial adaptive parameter values, and projection boundaries. An empirical approach that assumes that the control parameters reach their ideal values within three time constants is employed to determine the adaptation rates [49,50]. This method can mathematically be expressed as

$$\Gamma_{\Theta_{ii}} = \frac{\|\Theta_i\|}{3\tau_m |r_m^2|} \tag{88}$$

where τ_m is the smallest time constant of the reference model A_m and r_m is the maximum value of the reference. Because the ideal control parameter values are unknown, the nominal ideal values (calculated using the nominal plant dynamics) are used instead. It is noted that Eq. (88) is mainly used as a starting point for fine-tuning the adaptation rates. The initial conditions of all the adaptive control parameters are set to 0. Finally, the projection boundaries are selected by observing the variation of controller parameters during simulations.

C. Stability Limits

As stated in Theorem III.2, once the DRCRM adaptive controller is designed as given in Eqs. (59) and (67–79), the stability of the overall system is determined by the roots of the characteristic polynomial presented in Eq. (85). We use the DDE-BIFTOOL (delay differential equation bifurcation tool) [51] to find the rightmost root, among infinitely many of them, of this polynomial for the simulation example. Specifically, we are interested in the effect of the operator parameters K_p and T_p in Eq. (87) on the stability of the overall system. Figure 5 shows the location of the rightmost root of the characteristic polynomial (85) for different values of K_p and T_p for a fixed human operator reaction time delay $\tau_h = 0.2$ s. The red areas in the figure represent the unstable regions. It can be argued that the system can be swept into the unstable region for moderately high values of T_p. In addition, the relatively small patch of instability around $K_p = 0.6$ and $T_p = 0.07$ shows the possibility of unexpected system behavior due to operator time delays.

D. Simulation Results

The flight simulations have been conducted by a model reference adaptive controller (MRAC), a closed-loop reference model adaptive controller (CRM), and a delay-resistant closed-loop reference model adaptive controller. Overall closed-loop control systems are labeled as MRAC-H, CRM-H, and DRCRM-H, respectively, where the letter H represents the presence of a human operator.

Tracking performances of a MRAC-H controller for different input delays is presented in Fig. 6. It is observed that the position tracking deteriorates after the injection of the anomaly at $t = 16$ s, and this deterioration becomes unacceptable as the plant time delay τ_s increases beyond 0.10 s, for example, at $\tau_s = 0.18$ s. Figures 7 and 8 show the tracking performances and the control inputs of MRAC-H, CRM-H, and DRCRM-H configurations for $\tau_s = 0.10$ s. The figures show that, although a CRM-H based configuration provides a substantially more damped response in comparison to MRAC-H, DRCRM-H outperforms all the controllers in terms of position tracking and control energy spending. The effect of human operator reaction lags and control input delays can also be observed from the figures as delayed responses to commanded inputs.

Overall performance of different configurations, which is defined by the metric

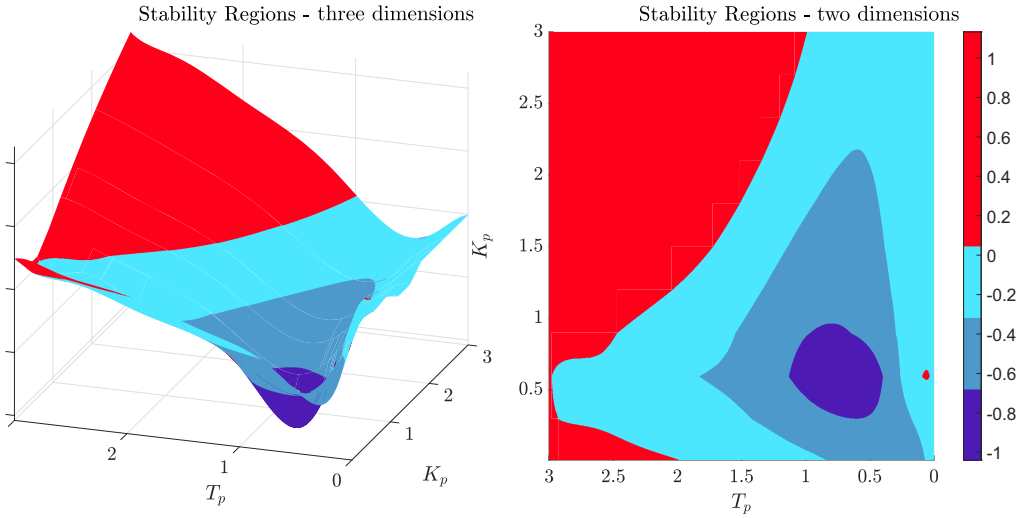

Fig. 5 Variation of rightmost pole location with respect to simultaneous change in K_p and/or T_p. ©[2021] Institute of Electrical and Electronics Engineers. Reprinted and updated, with permission, from E. Eraslan and Y. Yildiz, "Modeling and Adaptive Control of Flexible Quadrotor UAVs," *60th IEEE Conference on Decision and Control (CDC)*, Institute of Electrical and Electronics Engineers, Austin, TX, 2021, pp. 1783–1788.

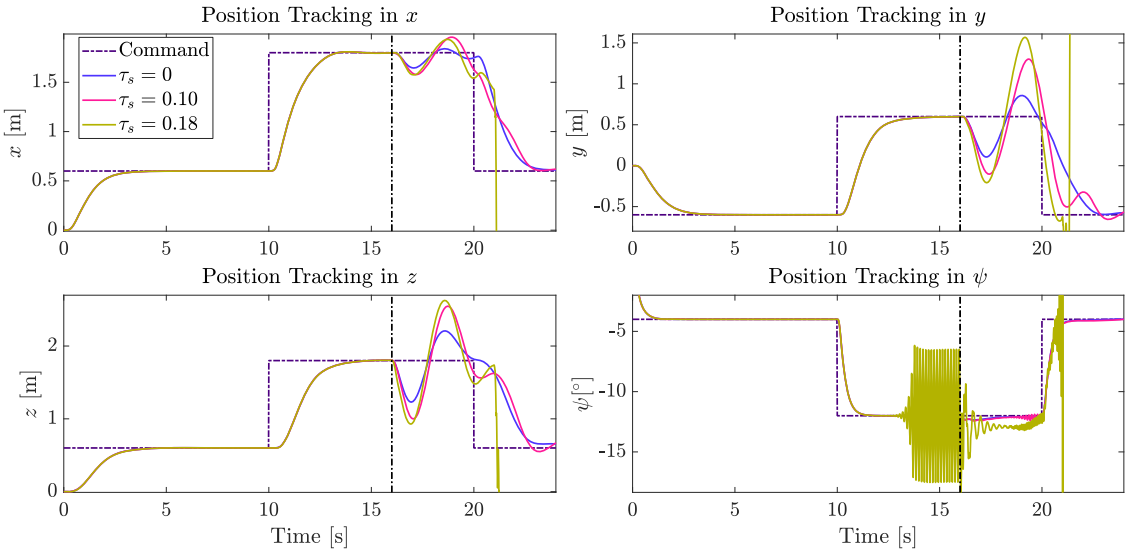

Fig. 6 The position tracking performance of the MRAC-H configuration for different input delays τ_s.

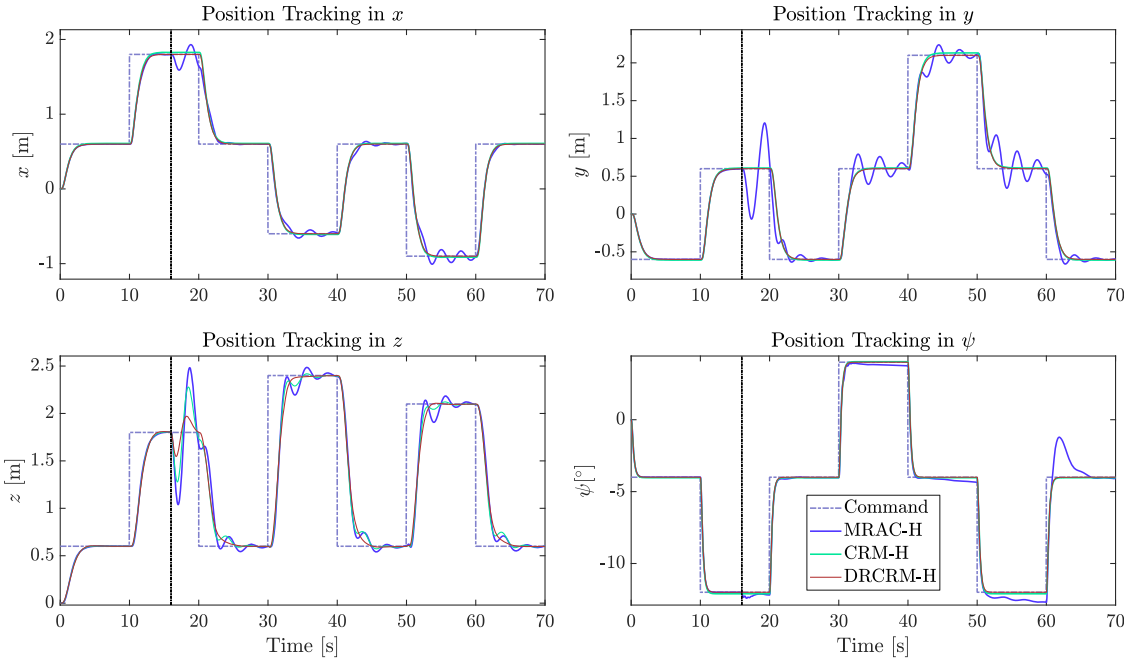

Fig. 7 The position tracking performance of the MRAC-H, CRM-H, and DRCRM-H configurations, for $\tau_s = 0.10$ s.

$$\mathcal{M}_e = \text{rms}(e(t))|_{t_a}^{T} \tag{89}$$

where $e(t)$ is the reference model tracking error, is provided in Table 1. As expected, the controller based on DRCRM-H provides better tracking performances. It is noted that the time interval is taken as the whole simulation time, which results in small error values. Therefore, percentage improvements, rather than absolute value differences, should be taken into account for comparisons.

The arm tip oscillations of the quadrotor for the tracking task given in Fig. 8 are shown in Fig. 9. MRAC-H configuration is susceptible to large amplitude oscillations throughout the simulation. While the CRM-H configuration manages to decrease these oscillations considerably at some regions, it is observed that the DRCRM-H configurations has the least amount of oscillations by tackling the time delays effectively, which could be predicted from the quadrotor trajectories provided in Fig. 7. Figure 10 shows the fast Fourier transform of arm tip oscillations, where it is seen that the DRCRM-H configuration produces the least vibration power.

In this study, we assumed that the quadrotor is build using polyethylene terephthalate glycol material, and using the properties of this material and Eq. (35), we calculated the first fundamental frequency as 131 Hz. Figure 11 shows that none of the controller signals has any significant excitation around this frequency, for the tracking task given in Fig. 7. The largest control effort is spent for the thrust channel, where DRCRM-H has the least control energy consumption.

Variation of the adaptive parameters under the effect of reference changes and anomalies is presented in Fig. 12. The horizontal dashed black lines in the subfigures denote the projection boundaries. Yellow bands are projection tolerance regions. In particular, CRM-H and DRCRM-H controllers adapt faster without any excessive oscillations. It is noted that the adaptation rates used in all of the control configurations are kept the same. Thanks to the projection operator, all control parameters remain within specified bounds.

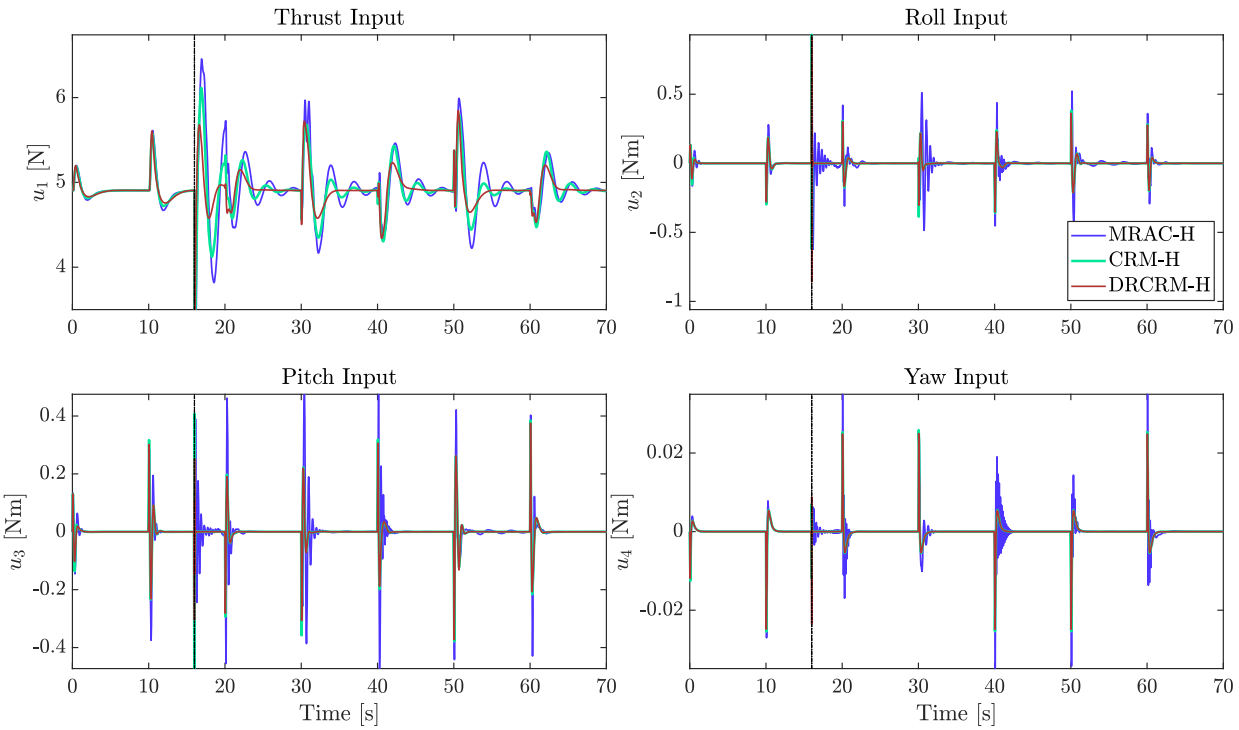

Fig. 8 The control inputs of the MRAC-H, CRM-H, and DRCRM-H configurations, for $\tau_s = 0.10$ s.

Table 1 The tracking performance assessment metric for the MRAC-H, CRM-H, and DRCRM-H configurations

Axes	$\mathcal{M}_e^{\text{MRAC-H}}$	$\mathcal{M}_e^{\text{CRM-H}}$	$\mathcal{M}_e^{\text{DRCRM-H}}$
x	5.229	0.002	0.001
y	16.059	0.002	0.001
z	13.133	0.209	0.132
ψ	0.958	0.001	0.000

V. Conclusions

This paper introduces a complete model of a flexible quadrotor with uncertain dynamics in full detail. In addition, the authors conducted a human-in-the-loop stability analysis of the overall closed-loop control system, consisting of the flexible UAV model with input delay, operator model with reaction time delay, and a delay-resistant closed-loop reference model adaptive controller. They further elaborate on the controller design for two different cases: a predefined reference input and real time operation. They demonstrate through careful comparative simulations, using the high-fidelity model they

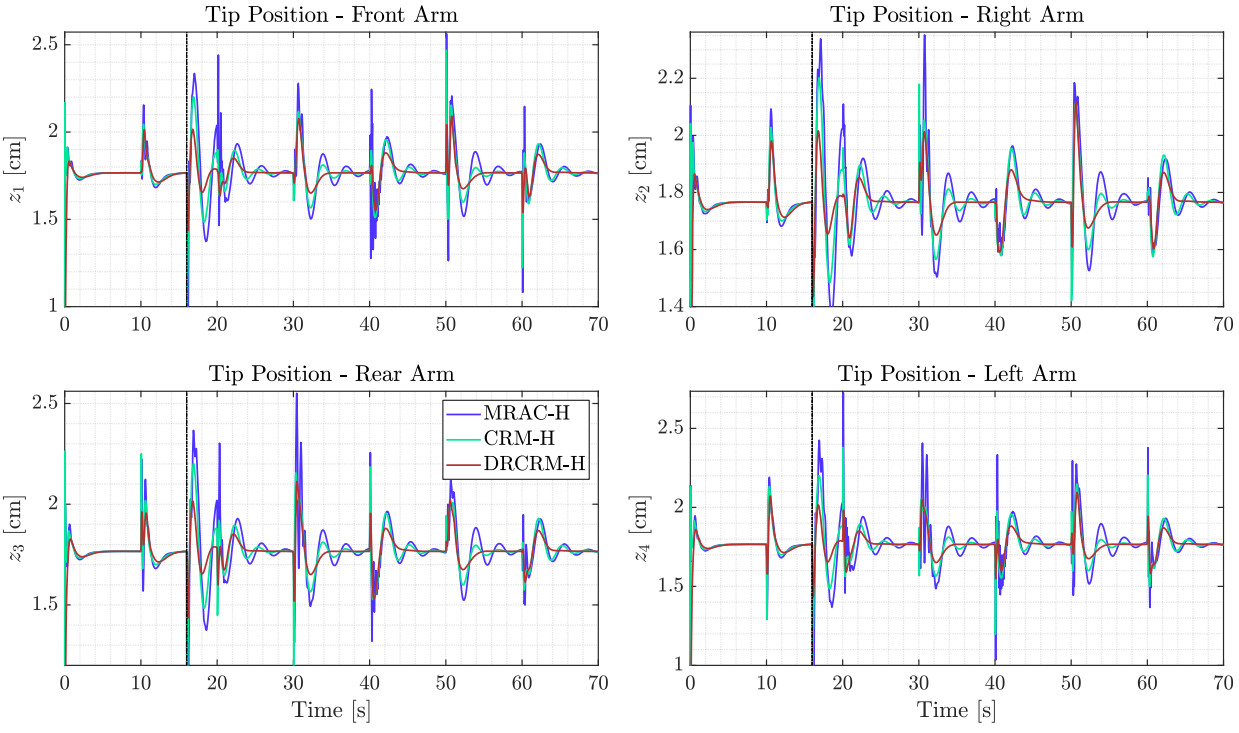

Fig. 9 The arm tip oscillations of the MRAC-H, CRM-H, and DRCRM-H configurations.

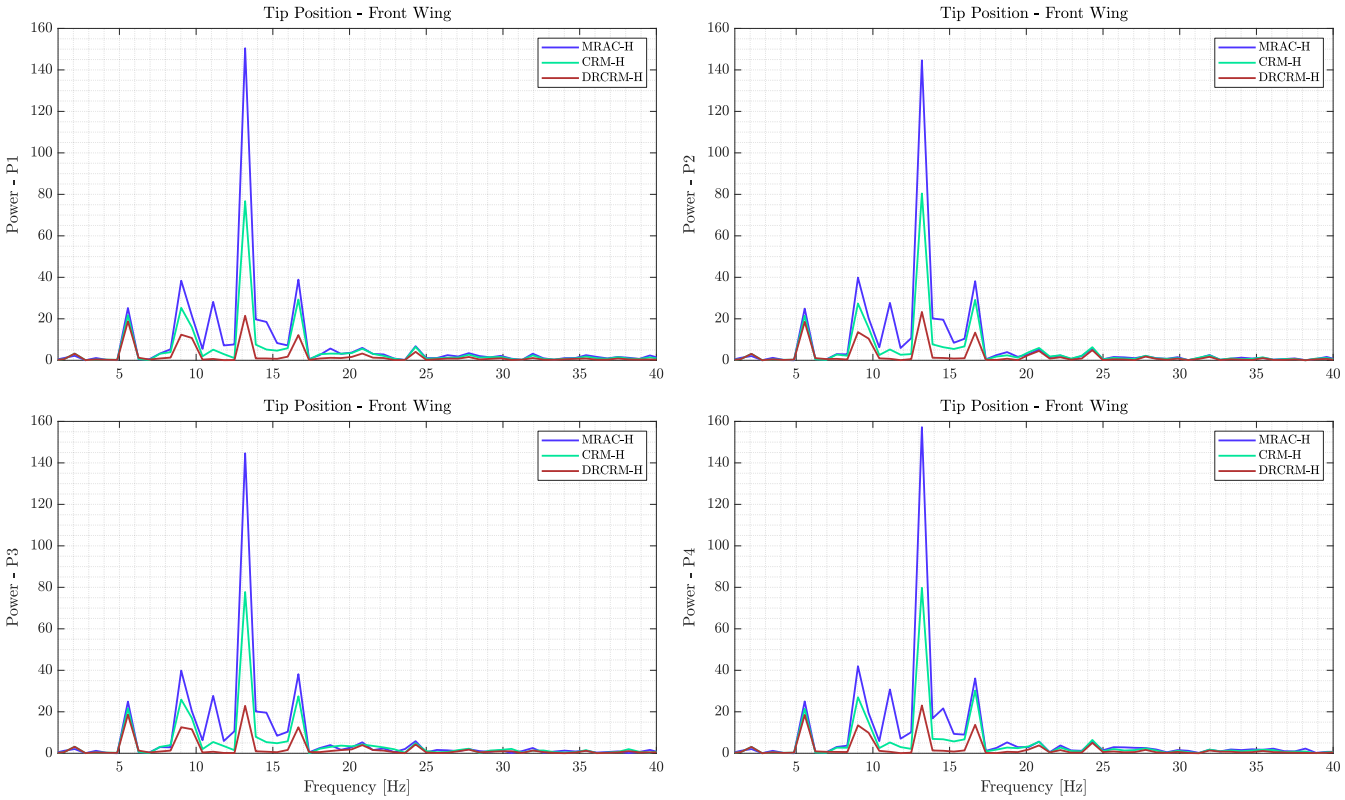

Fig. 10 The fast Fourier transform of the arm tip oscillations of the MRAC-H, CRM-H, and DRCRM-H configurations.

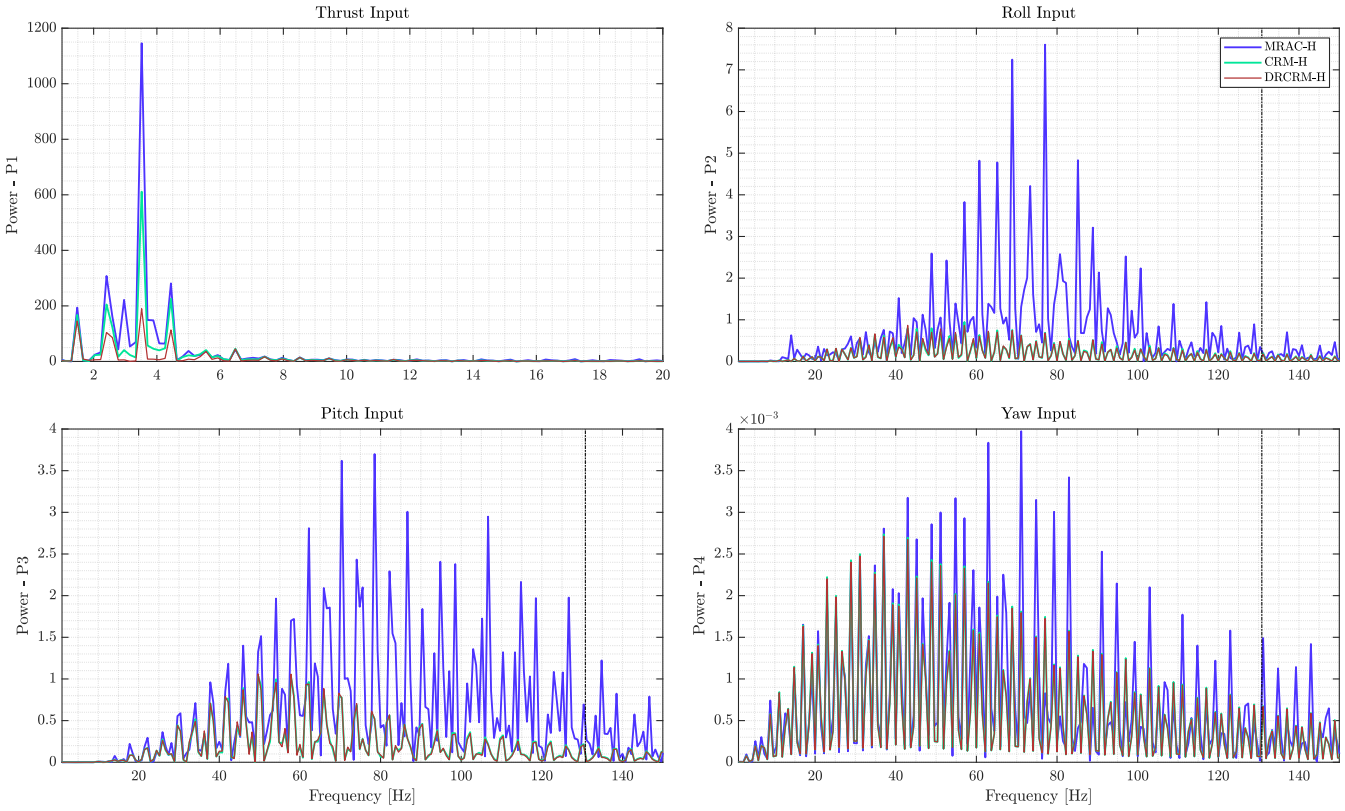

Fig. 11 The fast Fourier transform of the control inputs of the MRAC-H, CRM-H, and DRCRM-H configurations.

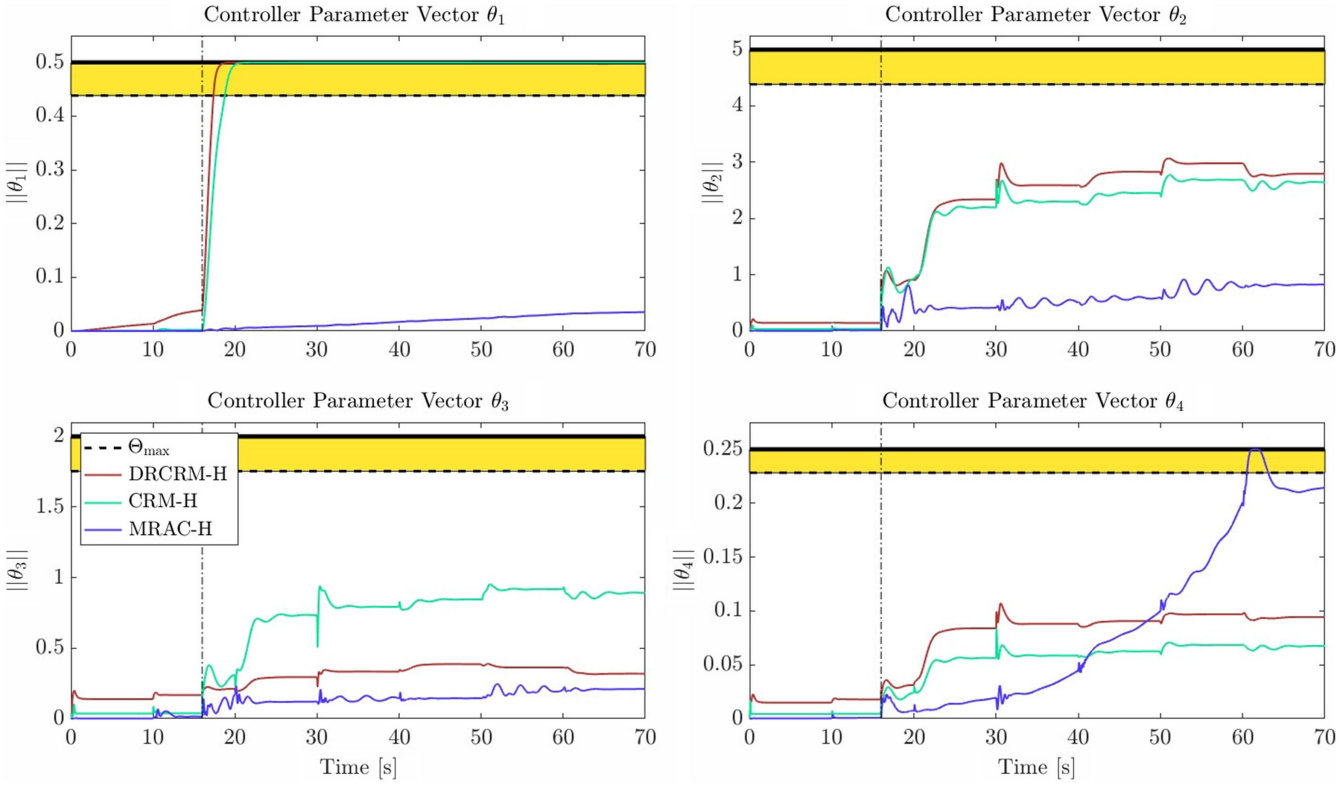

Fig. 12 The evolution of control parameters of the MRAC-H, CRM-H, and DRCRM-H configurations.

develop, that when DRCRM is employed in the presence of a human operator the resulting combination provides the most desirable performance with minimal oscillations compared to other alternative adaptive controllers.

Appendix A: Normalization Constant

Let

$$\bar{\beta}_j^* = \frac{\cos\bar{\beta}_j + \cosh\bar{\beta}_j}{\sin\bar{\beta}_j + \sinh\bar{\beta}_j} \tag{A1}$$

Substituting Eq. (A1) into Eq. (36), we obtain

$$W_j(\bar{x}) = \bar{\gamma}_j[(\cos\beta_j\bar{x} - \cosh\beta_j\bar{x}) - \bar{\beta}_j^*(\sin\beta_j\bar{x} - \sinh\beta_j\bar{x})] \tag{A2}$$

The normalization constant $\bar{\gamma}_j$ in Eq. (A2) can be calculated by the orthogonality of mode shape $W_j(\bar{x})$ as

$$\int_0^{L_c} \rho_c A_c W_j^2(\bar{x})\,\mathrm{d}\bar{x} = 1 \tag{A3}$$

$$\int_0^{L_c} \rho_c A_c \bar{\gamma}_j^2[(\cos\beta_j\bar{x} - \cosh\beta_j\bar{x}) - \bar{\beta}_j^*(\sin\beta_j\bar{x} - \sinh\beta_j\bar{x})]^2\,\mathrm{d}\bar{x} = 1 \tag{A4}$$

Solving Eq. (A4), the normalization constant is obtained as

$$\bar{\gamma}_j = \frac{1}{\sqrt{\rho_c A_c \gamma_c}} \tag{A5}$$

where

$$\begin{aligned}\gamma_c = \frac{1}{4\beta}[&-\bar{\beta}_j^{*2}\sin(2\bar{\beta}_j) + \bar{\beta}_j^{*2}\sinh(2\bar{\beta}_j) + 4\bar{\beta}_j^{*2}\cos(\bar{\beta}_j)\sinh(\bar{\beta}_j)\\ &- 4(\bar{\beta}_j^{*2}+1)\sin(\bar{\beta}_j)\cosh(\bar{\beta}_j) + 2\bar{\beta}_j^*\cos(2\bar{\beta}_j) - 2\bar{\beta}_j^*\cosh(2\bar{\beta}_j)\\ &+ 8\bar{\beta}_j^*\sin(\bar{\beta}_j)\sinh(\bar{\beta}_j) + 4\bar{\beta}_j + \sin(2\bar{\beta}_j) + \sinh(2\bar{\beta}_j)\\ &- 4\cos(\bar{\beta}_j)\sinh(\bar{\beta}_j)]\end{aligned} \tag{A6}$$

Appendix B: Application of Orthogonality Conditions

Recall that the partial differential equations of motion for a damped Euler–Bernoulli beam is given as

$$E_c J_c \frac{\partial^4 w(\bar{x},t)}{\partial\bar{x}^4} + \rho_c A_c \frac{\partial^2 w(\bar{x},t)}{\partial t^2} + \sigma_c \frac{\partial w(\bar{x},t)}{\partial t} = F(\bar{x},t) \tag{B1}$$

Using Eq. (5) and applying separation of variables, it can be obtained that

$$E_c J_c \frac{d^4 W_j(\bar{x})}{d\bar{x}^4} = \rho_c A_c \bar{\omega}_j^2 W_j(\bar{x}) \tag{B2}$$

Substituting Eq. (B2) into Eq. (B1) and using Eq. (5), it follows that

$$\rho_c A_c \bar{\omega}_j^2 W_j(\bar{x})\Upsilon_j(t) + \rho_c A_c W_j(\bar{x})\ddot{\Upsilon}_j(t) + \sigma_c W_j(\bar{x})\dot{\Upsilon}_j(t) = F(\bar{x},t) \tag{B3}$$

Recall that the orthogonality conditions can be written as

$$\int_0^{L_c} \rho_c A_c W_j(\bar{x}) W_l(\bar{x})\,\mathrm{d}\bar{x} = \delta_{jl} \tag{B4}$$

where δ_{jl} is the Kronecker delta. Multiplying Eq. (B3) by $W_l(\bar{x})$ and integrating it from 0 to L_c, it is obtained that

$$\sum_{j=1}^{\infty} \bar{\omega}_j^2 \Upsilon_j(t) \int_0^{L_c} \rho_c A_c W_j(\bar{x}) W_l(\bar{x})\,\mathrm{d}\bar{x} + \sum_{j=1}^{\infty} \ddot{\Upsilon}_j(t) \int_0^{L_c} \rho_c A_c W_j(\bar{x}) W_l(\bar{x})\,\mathrm{d}\bar{x} + \frac{\sigma_c}{\rho_c A_c} \sum_{j=1}^{\infty} \dot{\Upsilon}_j(t) \int_0^{L_c} \rho_c A_c W_j(\bar{x}) W_l(\bar{x})\,\mathrm{d}\bar{x} = \int_0^{L_c} W_l(\bar{x}) F(\bar{x}, t)\,\mathrm{d}\bar{x} \tag{B5}$$

In view of the orthogonality conditions given by Eq. (B4), it is obtained that

$$\ddot{\Upsilon}_j(t) + \sigma_c' \dot{\Upsilon}_j(t) + \bar{\omega}_j^2 \Upsilon_j(t) = \int_0^{L_c} W_j(\bar{x}) F(\bar{x}, t)\,\mathrm{d}\bar{x} \tag{B6}$$

where $\sigma_c' = \sigma_c/(\rho_c A_c)$ is a constant.

Acknowledgments

The authors would like to express their gratitude for the support of the Scientific and Technological Research Council of Turkey under grant number 118E937.

References

[1] Srikanth, M., Annaswamy, A., and Lavretsky, E., "Dynamic Modeling and Control of a Flexible Four-Rotor UAV," *AIAA Guidance, Navigation, and Control Conference*, AIAA Paper 2010-8050, 2010. https://doi.org/10.2514/6.2010-8050

[2] Verbeke, J., and Debruyne, S., "Vibration Analysis of a UAV Multirotor Frame," *Proceedings of ISMA. 2016 International Conference on Noise and Vibration Engineering*, ISMA, Leuven, Belgium, 2016, pp. 2401–2409.

[3] Tullu, A., Byun, Y., Kim, J. N., and Kang, B. S., "Parameter Optimization to Avoid Propeller-Induced Structural Resonance of Quadrotor Type Unmanned Aerial Vehicle," *Composite Structures*, Vol. 193, June 2018, pp. 63–72. https://doi.org/10.1016/j.compstruct.2018.03.014

[4] Rasti, A., and Fazelzadeh, S., "Multibody Dynamic Modeling and Flutter Analysis of a Flexible Slender Vehicle," *International Journal of Structural Stability and Dynamics*, Vol. 12, No. 6, 2012, Paper 1250049. https://doi.org/10.1142/S0219455412500496

[5] Meirovitch, L., and Nelson, H. D., "On the High-Spin Motion of a Satellite Containing Elastic Parts," *Journal of Spacecraft and Rockets*, Vol. 3, No. 11, 1966, pp. 1597–1602. https://doi.org/10.2514/3.28713

[6] Waszak, M. R., and Schmidt, D. K., "Flight Dynamics of Aeroelastic Vehicles," *Journal of Aircraft*, Vol. 25, No. 6, 1988, pp. 563–571. https://doi.org/10.2514/3.45623

[7] Flatus, D. H., "Aeroelastic Stability of Slender, Spinning Missiles," *Journal of Guidance, Control, and Dynamics*, Vol. 15, No. 1, 1992, pp. 144–151. https://doi.org/10.2514/3.20812

[8] Waszak, M. R., Davidson, J. B., and Schmidt, D. K., "A Simulation Study of the Flight Dynamics of Elastic Aircraft. Volume 1: Experiment, Results and Analysis," NASA-CR-4102, 1987.

[9] Baghdadi, N., Lowenberg, M. H., and Isikveren, A. T., "Analysis of Flexible Aircraft Dynamics Using Bifurcation Methods," *Journal of Guidance, Control, and Dynamics*, Vol. 34, No. 3, 2011, pp. 795–809. https://doi.org/10.2514/1.51468

[10] Da Ronch, A., Badcock, K., Wang, Y., Wynn, A., and Palacios, R., "Nonlinear Model Reduction for Flexible Aircraft Control Design," *AIAA Atmospheric Flight Mechanics Conference*, AIAA Paper 2012-4404, 2012. https://doi.org/10.2514/6.2012-4404

[11] Chang, C. S., Hodges, D. H., and Patil, M. J., "Flight Dynamics of Highly Flexible Aircraft," *Journal of Aircraft*, Vol. 45, No. 2, 2008, pp. 538–545. https://doi.org/10.2514/1.30890

[12] Nguyen, N., and Tuzcu, I., "Flight Dynamics of Flexible Aircraft with Aeroelastic and Inertial Force Interactions," *AIAA Atmospheric Flight Mechanics Conference*, AIAA Paper 2009-6045, 2009. https://doi.org/10.2514/6.2009-6045

[13] Van Schoor, M. C., and von Flotow, A. H., "Aeroelastic Characteristics of a Highly Flexible Aircraft," *Journal of Aircraft*, Vol. 27, No. 10, 1990, pp. 901–908. https://doi.org/10.2514/3.45955

[14] Ritter, M., Jones, J., and Cesnik, C. E., "Enhanced Modal Approach for Free-Flight Nonlinear Aeroelastic Simulation of Very Flexible Aircraft," *15th Dynamics Specialists Conference*, AIAA Paper 2016-1794, 2016. https://doi.org/10.2514/6.2016-1794

[15] Cesnik, C., Senatore, P., Su, W., Atkins, E., Shearer, C., and Pitchter, N., "X-HALE: A Very Flexible UAV for Nonlinear Aeroelastic Tests," *51st AIAA/ASME/ASCE/AHS/ASC Structures, Structural Dynamics, and Materials Conference 18th AIAA/ASME/AHS Adaptive Structures Conference 12th*, AIAA Paper 2010-2715, 2010. https://doi.org/10.2514/6.2010-2715

[16] Sanz, R., Garcia, P., Zhong, Q.-C., and Albertos, P., "Predictor-Based Control of a Class of Time-Delay Systems and Its Application to Quadrotors," *IEEE Transactions on Industrial Electronics*, Vol. 64, No. 1, 2016, pp. 459–469. https://doi.org/10.1109/TIE.2016.2609378

[17] Cao, N., and Lynch, A. F., "Predictor-Based Controllers for UAVs with Input Delay," *2017 IEEE International Conference on Advanced Intelligent Mechatronics (AIM)*, Inst. of Electrical and Electronics Engineers, New York, 2017, pp. 803–808. https://doi.org/10.1109/AIM.2017.8014116

[18] Wang, Q., Wang, J.-W., Yu, Y., and Sun, C.-Y., "Robust Attitude Control of an Indoor Micro Quadrotor with Input Delay," *Proceedings of 2014 IEEE Chinese Guidance, Navigation and Control Conference*, Inst. of Electrical and Electronics Engineers, New York, 2014, pp. 2363–2368. https://doi.org/10.1109/CGNCC.2014.7007538

[19] Wang, J., Zhou, Z., Wang, C., and Ding, Z., "Cascade Structure Predictive Observer Design for Consensus Control with Applications to UAVs Formation Flying," *Automatica*, Vol. 121, Nov. 2020, Paper 109200. https://doi.org/10.1016/j.automatica.2020.109200

[20] Alan, A., Yildiz, Y., and Poyraz, U., "High-Performance Adaptive Pressure Control in the Presence of Time Delays: Pressure Control for use in Variable-Thrust Rocket Development," *IEEE Control Systems Magazine*, Vol. 38, No. 5, 2018, pp. 26–52. https://doi.org/10.1109/MCS.2018.2851009

[21] Eraslan, E., Yildiz, Y., and Annaswamy, A. M., "Shared Control Between Pilots and Autopilots: Illustration of a Cyber-Physical Human System," *IEEE Control Systems Magazine*, Vol. 40, No. 6, 2020, pp. 79–99. https://doi.org/10.1109/MCS.2020.3019721

[22] Eraslan, E., "Shared Control in Aerial Cyber-Physical Human Systems," Master's Thesis, Bilkent Univ., Türkiye, 2021,

[23] Annaswamy, A. M., and Yildiz, Y., "Cyber-Physical-Human Systems," *Encyclopedia of Systems and Control*, Springer–Verlag, Berlin, 2021, pp. 497–508. https://doi.org/10.1007/978-3-030-44184-5_100113

[24] Albaba, B. M., and Yildiz, Y., "Modeling Cyber-Physical Human Systems via an Interplay Between Reinforcement Learning and Game Theory," *Annual Reviews in Control*, Vol. 48, Jan. 2019, pp. 1–21. https://doi.org/10.1016/j.arcontrol.2019.10.002

[25] Eraslan, E., and Yildiz, Y., "Modeling and Adaptive Control of Flexible Quadrotor UAVs," *60th IEEE Conference on Decision and Control (CDC)*, Inst. of Electrical and Electronics Engineers, Austin, TX, 2021, pp. 1783–1788. https://doi.org/10.1109/CDC45484.2021.9683103

[26] Bauchau, O. A., and Craig, J. I., *Structural Analysis: with Applications to Aerospace Structures*, Vol. 163, Springer Science & Business Media, Berlin, 2009, pp. 560–575. https://doi.org/10.1007/978-90-481-2516-6

[27] Vepa, R., *Flight Dynamics, Simulation, and Control: For Rigid and Flexible Aircraft*, CRC Press, Boca Raton, FL, 2023, pp. 489–493. https://doi.org/10.1201/9781003266310

[28] Stengel, R. F., *Flight Dynamics*, Princeton Univ. Press, Princeton, NJ, 2005, pp. 147–150. https://doi.org/10.1515/9781400866816

[29] Vinh, N. X., *Flight Mechanics of High-Performance Aircraft*, Vol. 4, Cambridge Univ. Press, Cambridge, England, U.K., 1993, pp. 11–20.

[30] Hesse, H., Palacios, R., and Murua, J., "Consistent Structural Linearization in Flexible Aircraft Dynamics with Large Rigid-Body Motion," *AIAA Journal*, Vol. 52, No. 3, 2014, pp. 528–538. https://doi.org/10.2514/1.J052316

[31] Schmidt, L. V., *Introduction to Aircraft Flight Dynamics*, AIAA, Reston, VA, 1998, pp. 100–105.

[32] Dussart, G., Portapas, V., Pontillo, A., and Lone, M., "Flight Dynamic Modelling and Simulation of Large Flexible Aircraft," *Flight Physics-*

Models, Techniques and Technologies, IntechOpen, London, U.K., 2018, pp. 49–72.
https://doi.org/10.5772/intechopen.68297

[33] Mahmoodi, S., Khadem, S., and Kokabi, M., "Non-Linear Free Vibrations of Kelvin–Voigt Visco-Elastic Beams," *International Journal of Mechanical Sciences*, Vol. 49, No. 6, 2007, pp. 722–732.
https://doi.org/10.1016/j.ijmecsci.2006.10.005

[34] Romaszko, M., Sapiński, B., and Sioma, A., "Forced Vibrations Analysis of a Cantilever Beam Using the Vision Method," *Journal of Theoretical and Applied Mechanics*, Vol. 53, No. 1, 2015, pp. 243–254.
https://doi.org/10.15632/jtam-pl.53.1.243.

[35] Friswell, M. I., and Lees, A. W., "The Modes of Non-Homogeneous Damped Beams," *Journal of Sound and Vibration*, Vol. 242, No. 2, 2001, pp. 355–361.
https://doi.org/10.1006/jsvi.2000.3323

[36] Gürgöze, M., and Erol, H., "Dynamic Response of a Viscously Damped Cantilever with a Viscous End Condition," *Journal of Sound and Vibration*, Vol. 298, Nos. 1–2, 2006, pp. 132–153.
https://doi.org/10.1016/j.jsv.2006.04.042

[37] Rao, S. S., *Vibration of Continuous Systems*, Wiley, Hoboken, NJ, 2019, pp. 341–343.
https://doi.org/10.1002/9780470117866

[38] Gibson, T., Annaswamy, A., and Lavretsky, E., "Improved Transient Response in Adaptive Control Using Projection Algorithms and Closed Loop Reference Models," *AIAA Guidance, Navigation, and Control Conference*, AIAA Paper 2012-4775, 2012.
https://doi.org/10.2514/6.2012-4775

[39] Yildiz, Y., Annaswamy, A., Kolmanovsky, I. V., and Yanakiev, D., "Adaptive Posicast Controller for Time-Delay Systems with Relative Degree $n^* \leq 2$," *Automatica*, Vol. 46, No. 2, 2010, pp. 279–289.
https://doi.org/10.1016/j.automatica.2009.11.008

[40] Yildiz, Y., "Adaptive Control for Time Delay Systems Applied to Flight Control," *AIAA Guidance, Navigation, and Control Conference*, AIAA Paper 2010-7576, 2010.
https://doi.org/10.2514/6.2010-7576

[41] Duda, H., "Prediction of Pilot-in-the-Loop Oscillations Due to Rate Saturation," *Journal of Guidance, Control, and Dynamics*, Vol. 20, No. 3, 1997, pp. 581–587.
https://doi.org/10.2514/2.4080

[42] McRuer, D. T., and Jex, H. R., "A Review of Quasi-Linear Pilot Models," *IEEE Transactions on Human Factors in Electronics*, Vol. HFE-8, No. 3, 1967, pp. 231–249.
https://doi.org/10.1109/THFE.1967.234304

[43] Hess, R. A., "Prediction of Pilot Opinion Ratings Using an Optimal Pilot Model," *Human Factors*, Vol. 19, No. 5, 1977, pp. 459–475.
https://doi.org/10.1177/001872087701900503

[44] McRuer, D., and Schmidt, D. K., "Pilot-Vehicle Analysis of Multiaxis Tasks," *Journal of Guidance, Control, and Dynamics*, Vol. 13, No. 2, 1990, pp. 348–355.
https://doi.org/10.2514/3.20556

[45] Yucelen, T., Yildiz, Y., Sipahi, R., Yousefi, E., and Nguyen, N. T., "Stability Analysis of Human-Adaptive Controller Interactions," *AIAA Guidance, Navigation, and Control Conference*, AIAA Paper 2017-1493, 2017.
https://doi.org/10.2514/6.2017-1493

[46] Thurling, A. J., "Improving UAV Handling Qualities Using Time Delay Compensation," Ph.D. Dissertation, School of Engineering and Management, Air Force Inst. of Technology, Wright-Patterson AFB, Ohio, 2000.

[47] Witte, J. B., "An Investigation Relating Longitudinal Pilot-Induced Oscillation Tendency Rating to Describing Function Predictions for Rate-Limited Actuators," Ph. D. Dissertation, School of Engineering and Management, Air Force Inst. of Technology, Wright–Patterson AFB, 2004.

[48] Miller, C., "Nonlinear Dynamic Inversion Baseline Control Law: Architecture and Performance Predictions," *AIAA Guidance, Navigation, and Control Conference*, AIAA Paper 2011-6467, 2011.
https://doi.org/10.2514/6.2011-6467

[49] Dydek, Z., Jain, H., Jang, J., Annaswamy, A., and Lavretsky, E., "Theoretically Verifiable Stability Margins for an Adaptive Controller," *AIAA Guidance, Navigation, and Control Conference and Exhibit*, AIAA Paper 2006-6416, 2006.
https://doi.org/10.2514/6.2006-6416

[50] Yildiz, Y., Annaswamy, A. M., Yanakiev, D., and Kolmanovsky, I., "Spark Ignition Engine Fuel-to-Air Ratio Control: An Adaptive Control Approach," *Control Engineering Practice*, Vol. 18, No. 12, 2010, pp. 1369–1378.
https://doi.org/10.1016/j.conengprac.2010.06.011

[51] Engelborghs, K., Luzyanina, T., and Roose, D., "Numerical Bifurcation Analysis of Delay Differential Equations Using DDE-BIFTOOL," *ACM Transactions on Mathematical Software*, Vol. 28, No. 1, 2002, pp. 1–21.
https://doi.org/10.1145/513001.513002